A parametric study of buoyancy-driven flow of two-immiscible fluids in a differentially heated inclined channel

Anil Bhaurao Wakale, K. Venkatasubbaiah[1] and Kirti Chandra Sahu[2]

[1] *Department of Mechanical and Aerospace Engineering, Indian Institute of Technology Hyderabad, Yeddumailaram 502 205, Telangana, India*

[2] *Department of Chemical Engineering, Indian Institute of Technology Hyderabad, Yeddumailaram 502 205, Telangana, India*

Abstract

The buoyancy-driven interpenetration of two immiscible fluids in a differentially heated inclined channel is investigated by solving the Navier-Stokes, the continuity and the energy equations along with Cahn-Hillard equation to track the interface. After conducting a grid convergence test, a parametric study is conducted to investigate the effects of Reynolds number, Bond number, Marangoni number, density ratio, viscosity ratio and temperature difference between the walls (ΔT) on flow dynamics and interfacial instability between two immiscible fluids. We found that increasing Reynolds number, Bond number, ΔT, density ratio and decreasing viscosity ratio destabilizes the flow dynamics by increasing the intensity of vortical structures and 'mixing' of the fluids. The flow dynamics of vortical structures are altered by the imposed temperature gradient between the walls in comparison with isother-

[1]Email: Tel: +91 40 2301 6074, Email: kvenkat@iith.ac.in

mal system. We found a critical Bo below which the surface tension force dominates the gravitational force for the set of parameter values considered, which in turn give rise to stationary stable interface.
Keywords: Buoyancy-driven flow, Immiscible flow, Interfacial instability, Multiphase flow, Mixing, Laminar flow.

---

1. Introduction

The interpenetration of two immiscible fluids in an confined inclined channel under the action of gravitational force is frequently encounter in many industrial and natural phenomena and thus has been investigated by several authors in the past, see for instance, [1–6]. Consider two immiscible fluids having different density and viscosity occupying the upper and lower half of an inclined channel and initially separated by a partition. At time, $t = 0$, the partition is suddenly removed and the fluids are allowed to mix by the action of the gravitational force. This problem is frequently referred to as the "lock-exchange" problem [3, 7–9]. This phenomenon not only plays an important role in the design of chemical and petroleum engineering processes [1, 2], but also helps in understanding various natural systems in oceanography and atmospheric sciences [10].

The "lock-exchange" problem (shown in figure 1) has been investigated experimentally [3, 11–14] and numerically [6, 7] by considering fluids having equal viscosity. However, viscosity differential between fluids can have significant effect on the dynamics of the unsteady mixing process, which was

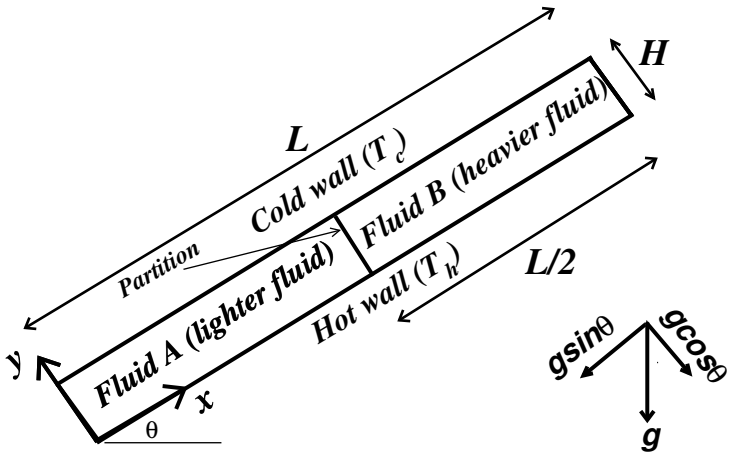

Figure 1: Schematic diagram (not to scale) showing the initial flow configuration when the bottom wall is hotter than the top wall. A heavier fluid (fluid 'B') is overlaying a lighter one (fluid 'A') in an inclined channel. They are initially separated by a partition, which is being removed at $t = 0$. θ is the tilt angle of the channel with the horizontal. The aspect ratio of the channel is $1 : 40$. The volume fraction of the lighter fluid, C, whose value can be taken to be 1 and 0 for the lighter and heavier fluids, respectively.

recently investigated by [5]. The dimensionless parameters characterizing the flow in this problem are density contrast characterized by Atwood number, $At \equiv (\rho_B - \rho_A)/(\rho_B + \rho_A)$, the tilt angle, θ (measured from horizontal) and the viscosity ratio of the two fluids, $\mu_r (\equiv \mu_B/\mu_A)$, wherein ρ_A, μ_A and ρ_B, μ_B are the densities and viscosities of fluids 'A' and 'B', respectively. It is important to note here that all the above mentioned studies are for isothermal systems, although in most of the industrial applications this phenomena encounter with temperature gradient between the fluids and also in geometry having differentially heated boundaries. This is the subject of the present investigation. However, we shall discuss the dynamics associated with the isothermal systems first before discussing the previous works on non-isothermal systems.

In isothermal "lock-exchange" flows [14], three types of flow regimes and mixing patterns were observed depending on the values of the tilt angle. In channel with tilt angles ($90^\circ \geq \theta \geq 25^\circ$), increasing θ decreases the magnitude of the front velocity of the high and low density fluids moving in the opposite directions. The front velocity (V_f) depends on the local density contrast across the interface. In this regime, flow and mixing are influenced by two distinct processes due to the components of the gravitational force along the axial and transverse directions of the channel. The former one accelerates the two fluids into each other at comparable velocities. During this motion, the interface separating the two fluids becomes unstable giving rise to the Kelvin-Helmholtz(KH) type instabilities, and consequent transverse mixing, which in turn decreases the front velocity. However, later one has an opposite effect by acting to segregate the two fluids and helps to increase the front velocity. For lower tilt angles ($25^\circ > \theta > 8^\circ$) the front velocity is nearly constant, with a value approximately equals to $0.7\sqrt{Atgd}$, where g is the gravitational acceleration and d is a characteristic dimension (diameter of the pipe in the study of [14]). For near horizontal channel ($\theta < 8^\circ$) the flow transitions to a third regime where the two fluids move as counter-current Poiseuille flows; the front velocity increases with increasing the value of the tilt angle. In this regime, the flow dynamics is a result of the balance between buoyancy and wall friction. Hallez and Magnaudet [7] numerically studied the buoyancy-induced mixing of two fluids in circular, rectangular and square geometries, and found that the flow dynamics are more coherent and persis-

tent in two than in three dimensions, which in turn give rise to more intense mixing and long-lasting flow structures in two-dimensional than in three dimensional geometries. Sahu and Vanka [6] investigated interpenetration of two immiscible fluids in a tilted channel using a lattice Boltzmann method (LBM). They conducted a parametric study by varying Atwood number, Reynolds number, tilt angle and surface tension. Their results compared well with the previous experimental results [3, 13, 14]. Nasr-Azadani *et al.*[15, 16] also studied the "lock-exchange" flows in the context of turbidity currents. Next we discuss the related works conducted on non-isothermal systems.

The influence of combined buoyancy and thermal convection in immiscible liquid layers occurs in many industrial applications, such as alloying techniques, processing of ceramics and semiconductors that frequently involves molten and gaseous phases. Several authors [17–21] investigated the effects the thermal convection in multiphase flows involving immiscible fluids by considering the temperature gradient along and normal to the interface. Prakash and Koster [19] studied thermal convection of two immiscible liquids in a container, which is differentially heated along the interface. They found that the flow pattern observed in their experiment agrees well with those obtained from their theoretical calculations. Liu *et al.* [18] numerically studied the thermocapillary convection in a rectangular channel having temperature gradient normal to the interface of two immiscible liquids in the context of crystal growth. They found that the flow structure and temperature field are symmetric with respect to interface. It was concluded that by adjusting

viscosity, conductivity of the fluids and thickness of the layers one could get desired flow patterns. Koster and Nguyen[22] showed that the appearance of two counter-rotating natural convection rolls in a system where the values of the temperature at the left and right walls lie below and above the density inversion temperature, or vice-versa. The unsteady laminar natural convection with internal heat generation in rectangular container with water as a working fluid and temperature gradient along the interface is investigated by [17]. The top and bottom walls are considered to be adiabatic. The effects of both heat generation and variations in the aspect ratio are investigated.

In spite of several studies those investigated thermal convection, to the best of our knowledge, mixing and interpenetration of two immisicible fluids in inclined channel with temperature gradient have not being investigated in literature. Also in most of the previous studies considered stable system with temperature gradient such that the lighter fluid overlays the heavier fluid. Hence the present investigation has been motivated to understand the interface deformation for unstable configuration (heavier fluid on the top of a lighter one) in an inclined channel having differentially heated walls.

The rest of the paper is organized as follows. The problem is formulated in Section 2; Section 3 presents the numerical method used in the present study. Results are presented in Section 4, where the effects of Reynolds number, temperature difference between the walls, Bond number, viscosity ratio, Marangoni number and density ratio on mixing and interfacial instability characteristics are provided. The concluding remarks are given in Section 5.

2. Formulation

We consider buoyancy-driven flow of two immiscible liquids in an inclined two-dimensional confined channel of length, L and height, H having differentially heated walls as shown in Fig. 1. The walls are considered to be rigid and impermeable. The walls at $x = (0, L)$ are insulated and the walls at $y = 0$ and $y = H$ are maintained at fixed values of temperature. Two cases are considered (i) when the bottom wall is hotter than the top wall, and (ii) the top wall is hotter than the bottom wall. T_c and T_h represent the temperature of the cold and hot walls, respectively, such that the temperature difference between the walls, $\Delta T = T_h - T_c$. The liquids are assumed to be Newtonain and incompressible. A rectangular coordinate system (x, y) is used to model the flow dynamics, where x and y denote the axial and transverse coordinates, respectively.

The flow dynamics is governed by continuity, incompressible Navier-Stokes equations along with energy equation. The diffuse interface method [4] is used to track the interface separating the immiscible fluids; the Cahn-Hillard equation for the volume fraction of the lighter fluid, C (whose value without losing generality can be taken to be 0 for the heavier fluid and 1 for the lighter fluid) is solved for this purpose.

The following scaling is employed to nondimensionalize the governing equations:

$$(x, y) = H\,(\widetilde{x}, \widetilde{y})\,,\ t = \frac{H}{V}\widetilde{t},\ (u, v) = V(\widetilde{u}, \widetilde{v}),\ p = \rho V^2 \widetilde{p},$$

$$\mu = \widetilde{\mu}\mu_A,\ \rho = \widetilde{\rho}\rho_A,\ \kappa = \widetilde{\kappa}\kappa_A,\ T = \widetilde{T}(T_h - T_c) + T_c, \tag{1}$$

where the tildes designate dimensionless quantities, V is the characteristic velocity, given by $\sqrt{gH}$; g being the acceleration due to gravity, μ_A, ρ_A and κ_A are the viscosity, the density and the thermal conductivity of fluid A (lighter fluid) at the reference temperature, T_c, respectively. After dropping tildes, the dimensionless governing equations are given by

$$\begin{aligned}
\nabla \cdot \mathbf{u} &= 0, && (2)\\
\rho\left[\frac{\partial \mathbf{u}}{\partial t} + \mathbf{u}\cdot\nabla\mathbf{u}\right] &= -\nabla p + \frac{1}{Re}\nabla\cdot\left[\mu(\nabla\mathbf{u} + \nabla\mathbf{u}^{\mathcal{T}})\right] + F, && (3)\\
\frac{\partial C}{\partial t} + \mathbf{u}\cdot\nabla C &= \frac{1}{Pe}\nabla\cdot(M\nabla\phi), && (4)\\
\frac{\partial T}{\partial t} + \mathbf{u}\cdot\nabla T &= \frac{1}{RePr}\nabla(\kappa\nabla T), && (5)
\end{aligned}$$

where $Re(\equiv \rho_A V H/\mu_A)$, $Bo(\equiv \rho_A g H^2/\sigma)$, $Pe(\equiv HV/M_c\phi_c)$, $Pr(\equiv \mu_A c_p/\kappa_A)$ denote Reynolds number, Bond number and Péclet number, Prandtl number, respectively, wherein M_c and ϕ_c are the characteristic values of mobility, M and chemical potential, respectively. In the above equations, $\mathbf{u} = (u, v)$ denotes the velocity field, wherein u and v represent the axial and transverse velocity components, respectively, p is the pressure field, t denotes time, and F is the combined body and surface forces per unit volume, which include the gravity and surface tension forces given by

$$F = \frac{\phi\nabla C}{Bo}(1 - \mathcal{M}T) - \rho\vec{j}, \tag{6}$$

where $\vec{j}$ represents the vertical direction (along the gravity), ϕ is chemical potential, given by $\epsilon^{-1}\sigma\alpha\psi' C - \epsilon\sigma\alpha\Delta C$, wherein $\psi(C) = C^2(1-C^2)/4$ is the bulk energy density, σ is the coefficient of surface tension, and ϵ is the measure of interface thickness, α is a constant [4]. The value of Péclet number is $O(1/\epsilon)$. The Marangoni number, $\mathcal{M}$ is given by $d\sigma/dT/\sigma_0$, σ_0 is the value of surface tension at the reference temperature.

The dimensionless density (ρ), viscosity (μ) and thermal conductivity (κ) are given by

$$\rho = C(1-\chi_A) + (1-C)\rho_r(1-\chi_B), \tag{7}$$

$$\mu = \left[C + (1-C)\mu_r\right] e^{-T}, \tag{8}$$

$$\kappa = C + (1-C)\kappa_r, \tag{9}$$

where ρ_r, μ_r and κ_r are the density ratio (ρ_B/ρ_A), viscosity ratio (μ_B/μ_A) and thermal conductivity ratio (κ_B/κ_A), respectively. The subscripts A and B correspond to the lighter and heavier fluids, respectively. As the fluids 'A' and 'B' are liquids, the viscosity decreases with increasing temperature, which is modelled as Eq. (8) [23]. χ_A and χ_B are given by $\beta_A\Delta T$ and $\beta_B\Delta T$, respectively, wherein using Boussinesq approximation β_A and β_B are defined as

$$\beta_{(A,B)} = -\frac{1}{\rho_{(A,B)}}\left(\frac{\partial\rho_{(A,B)}}{\partial T}\right)_p. \tag{10}$$

3. Numerical Method

A staggered grid finite-volume approach is incorporated in order to solve the system of equations (2)-(5). The scalar variables (the pressure, temperature and the volume fraction of the lighter fluid) are defined at the cell-centers and the velocity components are defined at at the cell faces, respectively. A weighted-essentially-non-oscillatory (WENO) scheme is used for discretization of the advective term in Eq. (4), and a central difference scheme is used to discretize the diffusive term. The Adams-Bashforth and the Crank-Nicholson methods are used for the advective and second-order dissipation terms in Eq. (3) in order to achieve second-order accuracy in the temporal discretization. In the solver, the no flow condition is prescribed at $t = 0$ and with the fluids at the reference temperature, T_c. The Cahn-Hillard equation (Eq. (4)) is first solved and the concentration filed is updated using the velocity field at previous time-steps (n^{th} step). The velocity field and temperature filed are then updated to next time step ($(n+1)^{th}$ step) by solving Eqs. (3) and (5) in conjunction with the continuity equation (Eq. (2)). This process is repeated as the time progress.

The systems of equations (2-5) are solved using no-slip and no-penetration boundary conditions at all the walls and the Neumann boundary conditions are imposed at the boundaries for concentration filed. The walls at $y = 0$ and $y = 1$ are maintained at the fixed values of temperature as mentioned in the formulation, and Neumann boundary conditions for temperature are used at the rest of the boundaries. The numerical method used in the present study

is similar to [4]. In a "lock-exchanged" isothermal flow system, we found that the velocity of the finger tip is $0.38\sqrt{AtgH}$ for smaller values of At, as considered in the present study. This result is similar to the finding obtained by Seon and co-workers [14]. However, we note that they considered circular tube in their experiment. The readers are also referred to the supplementary material of [24] for an extensive validation of the present code. We have ensured that convergence is indeed achieved upon mesh refinement, which is presented next.

3.1. Grid convergence test

In Fig. 2, the contours of the volume fraction of the lighter fluid, C for a typical set of parameters are plotted at $t = 40$ for different grids. It can be seen that the results for 2001×121 and 2562×66 are nearly the same. In view of this agreement obtained for the finer meshes, we opted to use 2562 and 66 grid points in the x and y directions, respectively to generate the rest of the results presented in this paper.

4. Results and discussion

4.1. Effect of Reynolds number

We begin the presentation of our results by studying the effects of Reynolds number. The spatio-temporal evaluations of the contours of the volume fraction of the lighter fluid, C are plotted for $Re = 100$ and $Re = 1000$ in Fig. 3(a) and (b), respectively. In each panel the results for configurations when

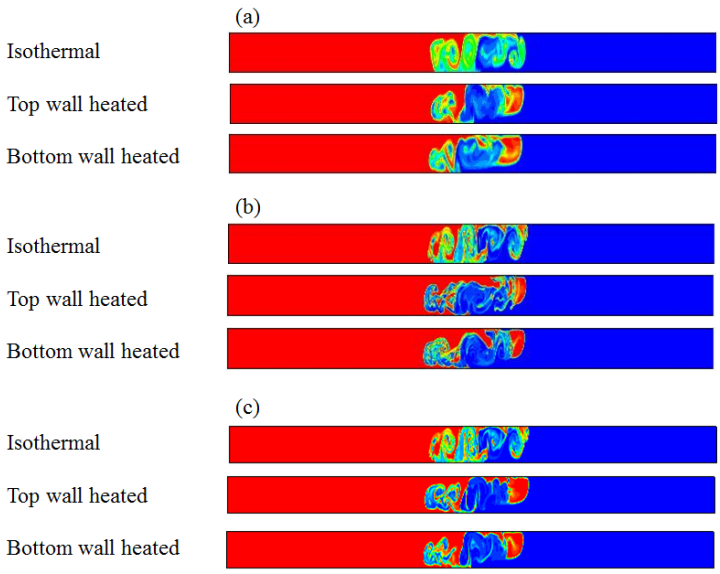

Figure 2: The contours of the volume fraction of the lighter fluid, C at $t = 40$ obtained using grids (a)701×41, (b) 2001×121 and (c) 2562×66. In each panels the top, middle and bottom sub-panels represent the results for isothermal, top-wall heated and bottom-wall heated cases, respectively. The rest of the parameter values are $Re = 1000$, $Bo = Re/0.01$, $Ma = 0.1$, $Pr = 4.34$, $\theta = 60°$, $\kappa_r = 4.36$, $\rho_r = 1.132$, $\mu_r = 0.0031$, and $\chi_A = \chi_B = 0.8$. Note that the values of χ_A and χ_B correspond to $\Delta T = 40°C$ for $\beta_1 = \beta_2 = 0.02$.

the top wall is heated and bottom wall is heated are plotted along with the isothermal case. It can be seen that due to the gravitational force acting in the axial direction, proportional to $gsin\theta$, the finger of the heavier fluid penetrates into the region of the lighter fluid in the negative axial (x) direction. In order to satisfy the conservation of mass the lighter fluid then moves in the positive x direction into the region of the heavier fluid. This motion of the heavier and lighter in the opposite directions leads to the development of mixed type of Kelvin-Helmholtz (KH) and Rayleigh-Taylor (RT) instabilities, which in turn give rise to the vortical structures. On the other hand,

the fluids are segregated due to the gravitational force acting in the transverse direction, proportional to $gcos\theta$. Thus the resultant complex dynamics observed in this figure is due to the competition of the gravitational force acting in the axial and transverse directions.

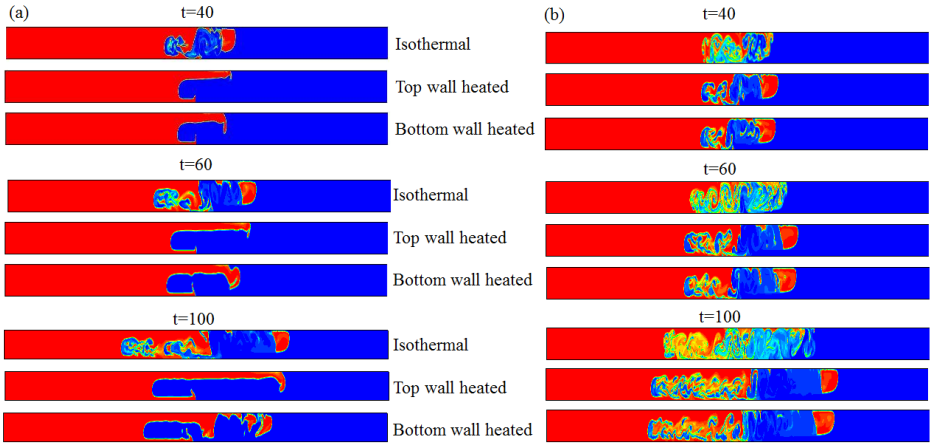

Figure 3: The spatio-temporal evaluation of contours of the volume fraction of the lighter fluid, C for (a) $Re = 100$ and (b) $Re = 1000$ at different times. In each panels the top, middle and bottom sub-panels represent the results for isothermal, top-wall heated and bottom-wall heated cases, respectively. The rest of the parameter values are $Bo = 10000$, $Ma = 0.1$, $Pr = 4.34$, $\theta = 60°$, $\kappa_r = 4.36$, $\rho_r = 1.132$, $\mu_r = 0.0031$, and $\chi_A = \chi_B = 0.8$. Note that the values of χ_A and χ_B correspond to $\Delta T = 40°C$ for $\beta_1 = \beta_2 = 0.02$.

Inspection of Fig. 3 reveals that the presence of heated wall, irrespective of the situations whether the top or bottom wall is heated, reduces the instabilities as compared to the isothermal case due to thermal convection. As expected, the comparison of the top and bottom wall heated cases shows that the flow dynamics is more unstable when the bottom wall is heated. This is due to the fact that when the bottom wall is hotter than the top wall, the fluids near the bottom wall becomes lighter and moves in the upward direc-

tion due to buoyancy, which enhances the interpenetration of the lighter fluid into the region of the heavier fluid in the transverse direction. It can also be seen that increasing Reynolds number increases the intensity of instabilities and formation of small-scale structures, which in turn increases the 'mixing' of the fluids. Close inspection of Fig. 3(a) also reveals that for lower value of Reynolds number at later times (see e.g $t = 100$) the speed of the heavier fluid is slower than that of the lighter fluid. This effect is more prominent for the top wall heated case. However, for $Re = 1000$ the inertial effects is significant and the asymmetrical effect observed for $Re = 100$, which arises due to thermal convection is minimized. Thus fingers of the heavier and lighter fluids move with almost at the same speed in the opposite direction as shown in Fig. 4. The corresponding axial and wall-normal velocity profiles at the finger tip of the heavier fluid at $t = 40$ and $t = 100$ are shown in Fig. 5. It can be seen that the velocity profiles show relatively more oscillations in the bottom wall heated case as compared to the top wall heated case due to buoyancy. As expected, it can be observed that the oscillations in the isothermal case are more as compared to non-isothermal flows. Also we found qualitatively the same features in the velocity profiles at the tip of the lighter fluid.

4.2. Effect of wall temperature

As the thermal convection is more for bottom-wall heated case, we considered only this case to investigate the effects of temperature difference between

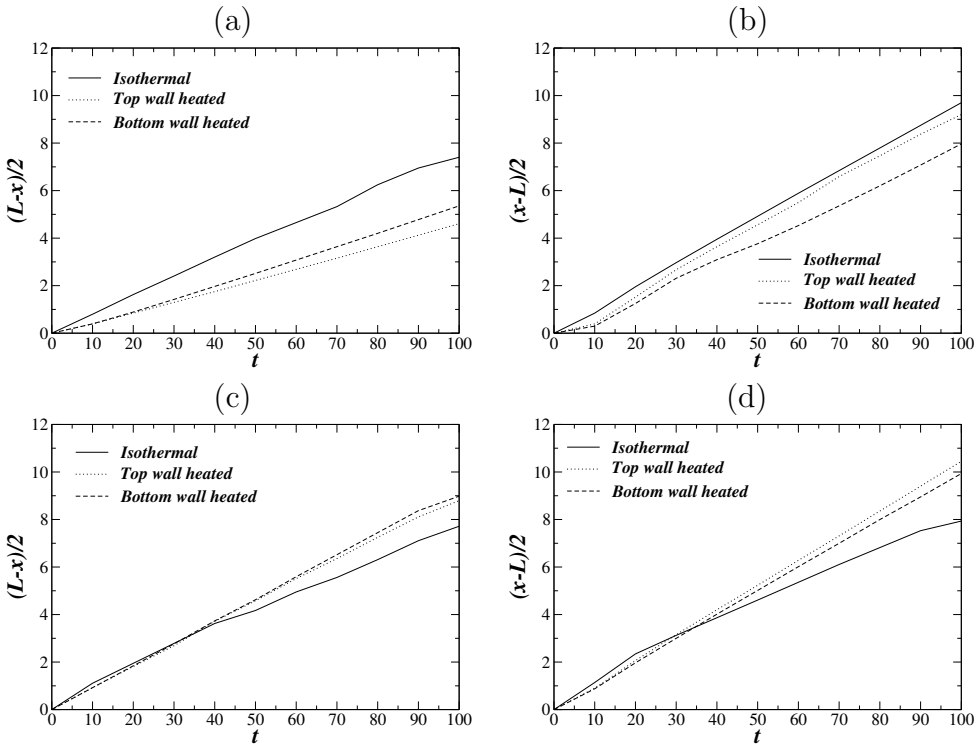

Figure 4: The distance travelled by the lighter, (a,c), and heavier (b,d) fronts, respectively. The panels (a,b) and (c,d) correspond to $Re = 100$ and $Re = 1000$, respectively. The rest of the parameter values are the same as those used to generate Fig. 3.

the top and bottom walls ($\Delta T(\equiv T_h - T_c)$). The spatio-temporal evaluations of C are plotted for $\chi_{(A,B)} = 0.02$ and 0.04, which correspond to $\Delta T = 20°C$ and $\Delta T = 40°C$ for $\beta = 10^{-3}$. It can be seen that due to the increase in buoyancy force with the increase in the temperature gradient between the walls, the intensity of the interfacial instabilities increases. Close inspection of Fig. 6 also reveals that increasing ΔT (i.e increasing buoyancy) increases the axial velocity of the fingers. Thus axial spreading length increases with increasing ΔT. The axial variations of the transverse averaged volume frac-

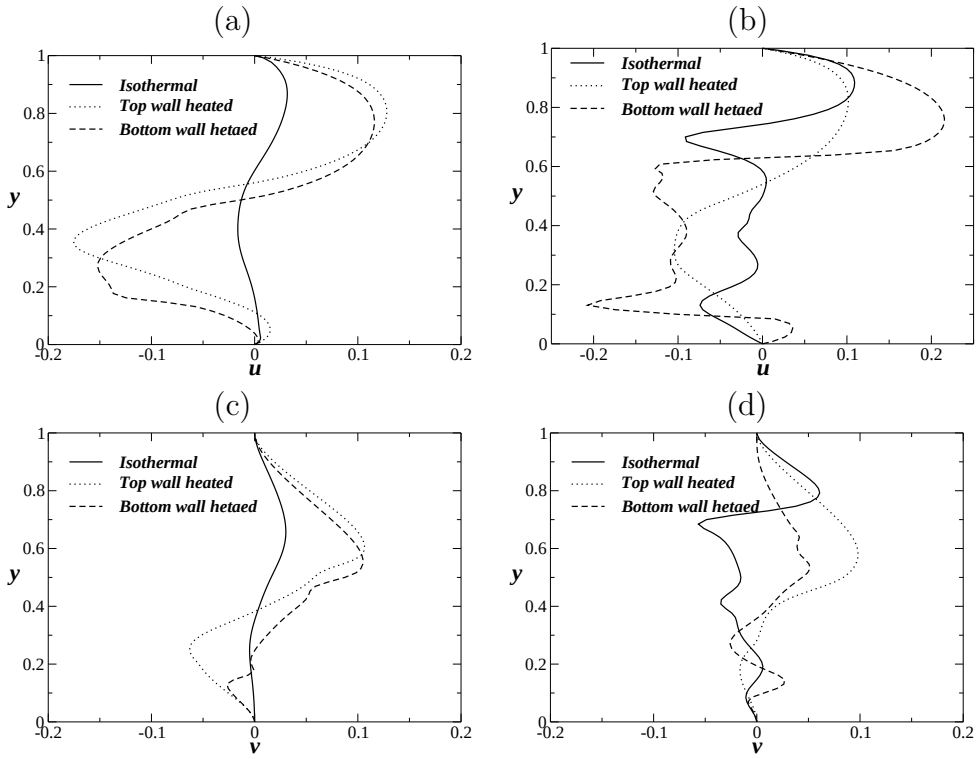

Figure 5: The axial (u) and the wall-normal (v) velocity profiles at the tip of the heavier fluid at (a,c) $t = 40$ and (b,d) $t = 100$, respectively for $Re = 1000$. The rest of the parameter values are the same as those used to generate Fig. 3.

tion of the lighter fluid, $\bar{C}_x$ for different values of ΔT are shown in Fig. 7(a), (b) and (c) at $t = 40$, 60 and 100, respectively. This plot shows that the spreading length increases with increasing in ΔT at every time. Close inspection also reveals that the variation of $\bar{C}_x$ becomes more chaotic for ΔT equals to $40°C$ as compared to $20°C$. The same features were also observed in Fig. 6.

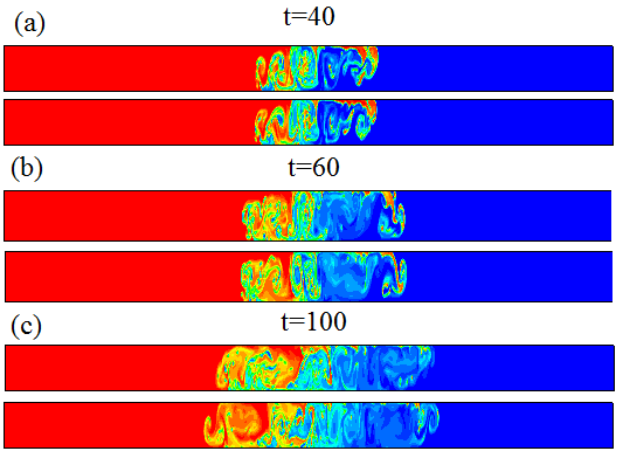

Figure 6: The spatio-temporal evaluation of contours of the volume fraction of the lighter fluid, C for different values wall temperature at (a) $t = 40$, (b) $t = 60$ and (c) $t = 100$. In each panels the top and bottom sub-panels represent the results for $\chi_{(A,B)} = 0.02$ (corresponds to $\Delta T = 20°C$) and $\chi_{(A,B)} = 0.04$ (corresponds to $\Delta T = 40°C$), respectively for $\beta_1 = \beta_2 = 0.001$. The rest of the parameter values are $Re = 1000$, $Bo = Re/0.01$, $Ma = 0$, $Pr = 7$, $\theta = 60°$, $\kappa_r = 4.36$, $\rho_r = 1.4$ and $\mu_r = 0.0031$.

4.3. Effect of surface tension

Next we investigate the effect of surface tension in Fig. 8, where the contours of the volume fraction of the lighter fluid, C are plotted for $Bo = 100$ and 1000 for isothermal, top-wall and bottom-wall heated cases. Increasing Bo means decreasing surface tension, if we keep the other scales the same. The rest of the parameter values are $Re = 1000$, $Ma = 0$, $Pr = 4.34$, $\theta = 60°$, $\kappa_r = 4.36$, $\rho_r = 1.132$ and $\mu_r = 0.0031$. It can be seen that for both the values of Bo considered the flow dynamics is more stable in case of non-isothermal systems as compared to that of the isothermal system. This is due to the fact that surface tension opposes the effect created by the gravitational force in the axial direction. Like the gravitational force in

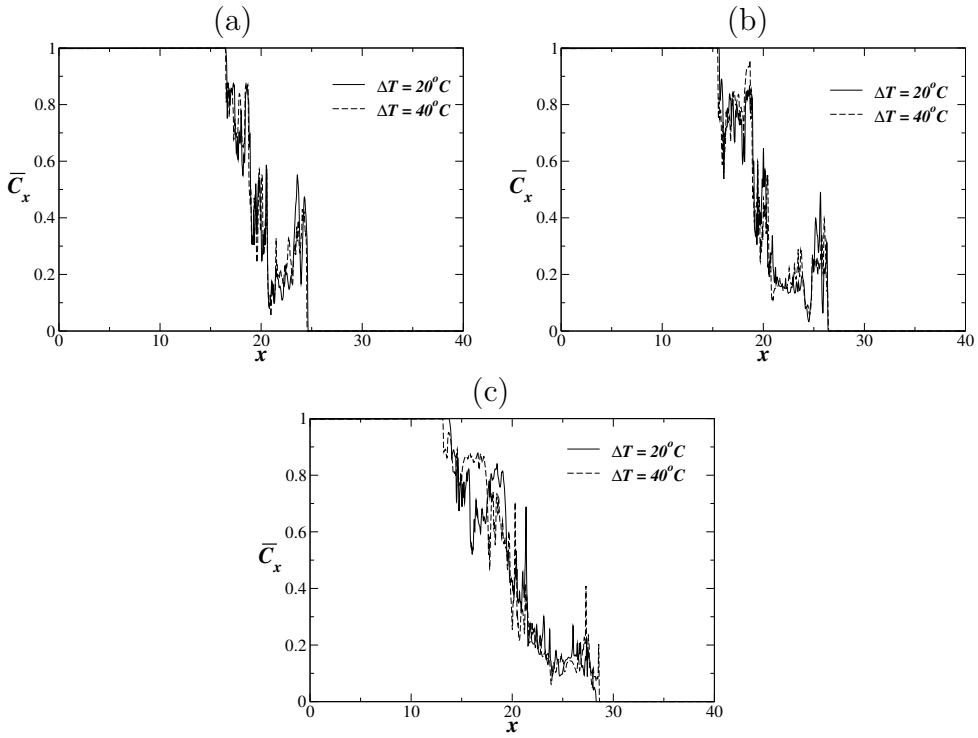

Figure 7: Variation of the transverse averaged volume fraction of the lighter fluid, $\bar{C}_x$ in the axial direction for different values ΔT at (a) $t = 40$, (b) $t = 60$ and (c) $t = 100$. The rest of the parameter values are the same as those used to generate Fig. 6.

the transverse direction, surface tension prevents the motion of the fingers in the opposite direction. It can be observed that the interface is almost stationary even at the later times (see Fig. 8(a)) for low value of Bo (high surface tension) considered. In this case the effects of surface tension and gravitational force in the transverse direction counterbalance with that of the axial component of the gravitational force. For $Bo = 1000$ (shown in Fig. 8(b)) the effect of surface tension is less as compared to $Bo = 100$ case (shown in Fig. 8(a)). Therefore although the interfacial instabilities appear, the intensity of these instabilities is much lower than those observed

in case of isothermal case. Close inspection also reveals that for higher Bo the axial prorogation of the fingers becomes asymmetrical, and as the lighter fluid moves into the region of the heavier fluid, a blob of the lighter fluid detached from the main finger, which moves in the upward direction almost independently from the main finger.

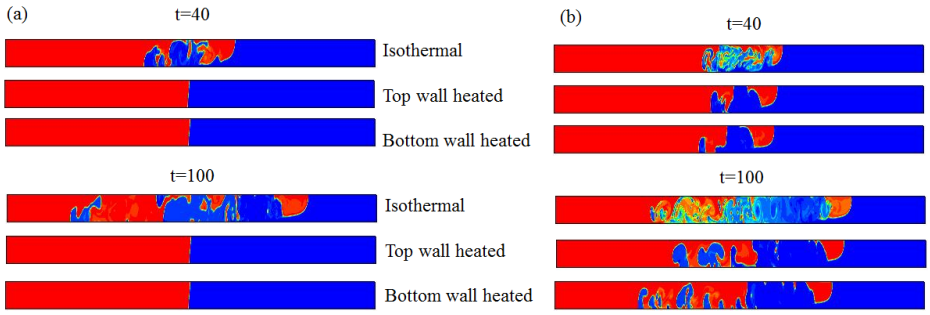

Figure 8: The contours of the volume fraction of the lighter fluid, C for different values Bond number at $t = 40$ and $t = 100$ for (a) $Bo = 100$ and (b) $Bo = 1000$. In each panels the top, middle and bottom sub-panels represent the results for isothermal, top-wall heated and bottom-wall heated cases, respectively. The rest of the parameter values are $Re = 1000$, $Ma = 0$, $Pr = 4.34$, $\theta = 60°$, $\kappa_r = 4.36$, $\rho_r = 1.132$, $\mu_r = 0.0031$ and $\Delta T = 40°C$

4.4. Effect of viscosity ratio

Then we investigate the effect of viscosity ratio. The contours of the volume fraction of the lighter fluid, C at $t = 100$ for $\mu_r = 0.01$, 0.1, 1 and 10 are plotted in Fig. 9(a), (b), (c) and (d), respectively. It is to be noted here that $\mu_r < 1$ ($\mu_r > 1$) represents the system where the heavier fluid is less (high) viscous. It can be seen that increasing viscosity ratio has a stabilizing influence. A similar finding was also observed by [25] in case of pressure-driven flow in an inclined channel. It can also be seen that for $\mu_r \leq 1$ a

blob of lighter fluid is detached from the main finger of the lighter fluid and moves independently. However, the dynamics is not observed for $\mu_r > 1$ (shown in Fig. 9(d)). The speed of the fingers is much lesser than that of the isothermal case for $\mu_r = 10$. In this case the flow structure becomes more like two individual Poiseuille flow and two stable fingers of the lighter and heavier fluids propagate in the upward and download directions, respectively. This behaviour is also evident in Fig. 10.

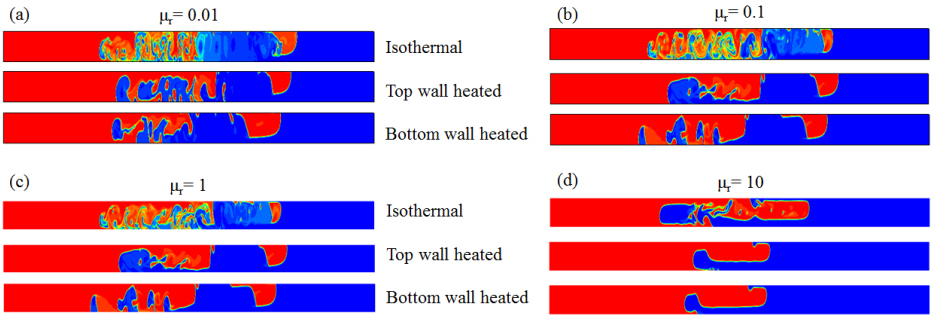

Figure 9: The contours of the volume fraction of the lighter fluid, C at $t = 100$ for (a) $\mu_r = 0.01$, (b) $\mu_r = 0.1$, (c) $\mu_r = 1$, (d) $\mu_r = 10$. In each panels the top, middle and bottom sub-panels represent the results for isothermal, top-wall heated and bottom-wall heated cases, respectively. The rest of the parameter values are $Re = 1000$, $Bo = 1000$, $Ma = 0$, $Pr = 4.34$, $\theta = 60°$, $\kappa_r = 4.36$, $\chi_A = \chi_B = 0.8$ $\rho_r = 1.132$ and $\mu_r = 0.0031$. Note that the values of χ_A and χ_B correspond to $\Delta T = 40°C$ for $\beta_1 = \beta_2 = 0.02$.

4.5. Effect of Marangoni number and density ratio

Finally we have investigated the effects of Marangoni number and density ratio in Fig. 11, where the contours of the volume fraction of the lighter fluid, C are plotted for isothermal case, $\mathcal{M} = 0$ and $\mathcal{M} = 0.3$ at $t = 50$. All the results presented in Fig. 11 correspond to the configuration when the bottom wall is heated. It can be seen that increasing the value of the

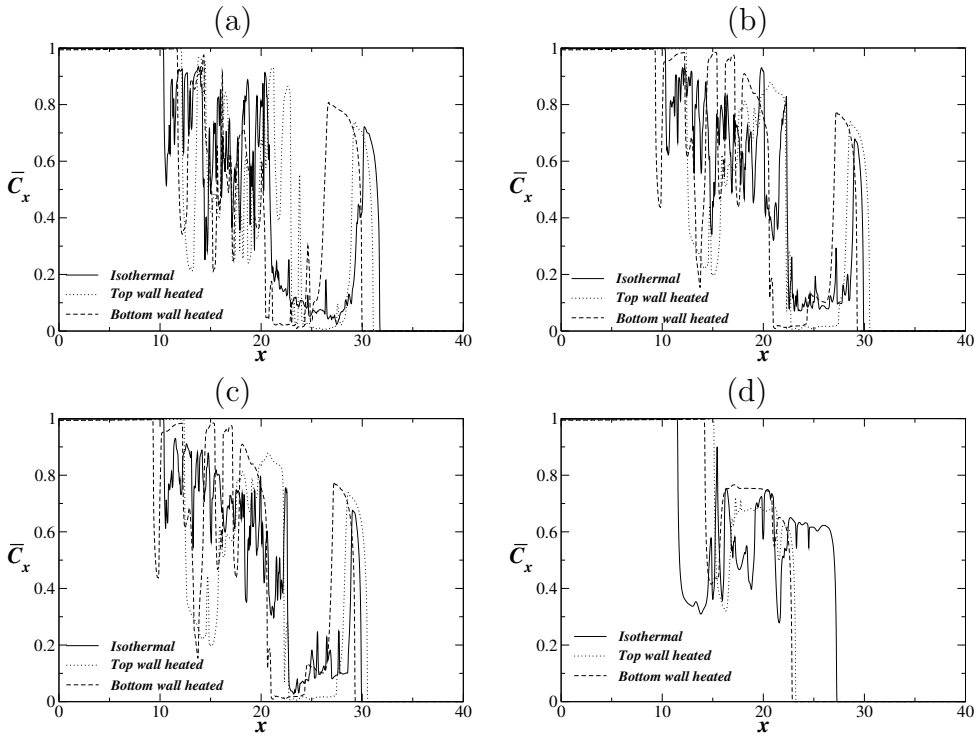

Figure 10: Variation of the transverse averaged volume fraction of the lighter fluid, $\bar{C}_x$ in the axial direction at $t = 100$ for (a) $\mu_r = 0.01$, (b) $\mu_r = 0.1$, (c) $\mu_r = 1$, (d) $\mu_r = 10$. The rest of the parameter values are the same as those used to generate Fig. 9.

Marangoni number slightly increases the speed of the propagating fingers and also increases the intensity of the instabilities and thereby increases the 'mixing' efficiency of the fluids. It can also be observed that increasing the density ratio increases the spreading for all the cases. This is expected because the speed of the fingers depends on the local density contrast across the interface. For density ratio, $\rho_r = 2$ it can be observed that the flow dynamics is completely dominated by the formation of the vortical structures which in turn give rise to intense 'mixing' of the fluids.

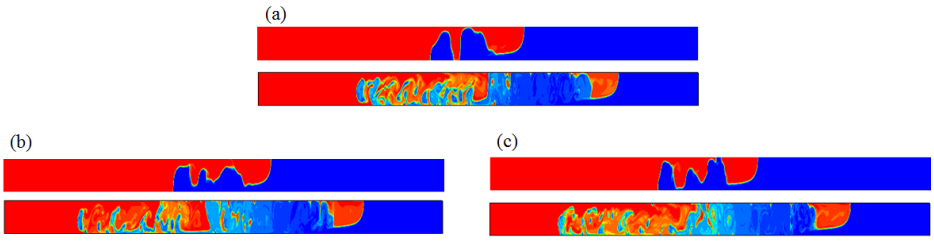

Figure 11: The contours of the volume fraction of the lighter fluid, C at $t = 50$ for (a) isothermal case, (b) $\mathcal{M} = 0$ and (c) $\mathcal{M} = 0.3$. In the figure all the results are generated for the bottom-wall heated case. In each panels the top and bottom sub-panels represent the results for $\rho_r = 1.131$ and $\rho_r = 2$. The rest of the parameter values are $Re = 200$, $Bo = 1000$, $Pr = 4.34$, $\theta = 60°$, $\chi_A = \chi_B = 0.04$, $\kappa_r = 4.36$ and $\mu_r = 0.0031$. Note that the values of χ_A and χ_B correspond to $\Delta T = 40°C$ for $\beta_1 = \beta_2 = 0.001$.

5. Concluding remarks

The buoyancy-driven interpenetration of two immiscible fluids in a differentially heated inclined channel is investigated via diffuse-interface based flow solver using finite-volume approach. The Navier-Stokes, continuity and energy equations are solved on a staggered grid along with Cahn-Hillard equation, which is now a well established method to handle immiscible fluids [4]. The effects of Reynolds number, Bond number, Marangoni number, density ratio, viscosity ratio and temperature difference between the walls (ΔT) have been investigated. The interfacial instability which is the combination of Kelvin-Helmholtz (KH) and Rayleigh-Taylor (RT) type instabilities have been observed due to motion of heavier and lighter fluids in the opposite direction. The flow dynamics and instability patterns in non-isothermal systems are very different as compared to those obtained in isothermal systems. The intensity of interfacial instabilities is very low as compared to those in

isothermal case for Re ≤ 100. This is due to thermal convection which acts to stabilize the flow. We found that increasing Reynolds number, Bond number, ΔT, density ratio and decreasing viscosity ratio destabilizes the flow dynamics by increasing the intensity of vortical structures and 'mixing' of the fluids. For $Bo \leq 100$ the flow dynamics is stable leading to stationary interface, as the gravity force balances the contour-acting surface tension force in non-isothermal flows. Although the effect of tilt angle of the channel with the horizontal has not be presented, we found that increasing the tilt angle increases the intensity of vortical structure and decreases the speed of the propagating finger. This behaviour was previously reported by [6].

References

[1] Benjamin TB. Gravity currents and related phenomena. J. Fluid Mech. 1968; 31:209-248.

[2] Joseph DD, Bai R, Chen KP, Renardy YY. Core-annular flows. Ann. Rev. Fluid Mech 1997;29:65-90.

[3] Debacq M, Hulin JP, Salin D, Perrin B, Hinch EJ. Buoyant mixing of miscible fluids of varying viscosities in vertical tubes. Phys. Fluids 2003;15:3846.

[4] Ding H, Spelt PDM, Shu C. Diffuse interface model for incompressible two-phase flows with large density ratios. J. Comput. Phys 2007;226;2078-2095.

[5] Redapangu PR, Vanka SP, Sahu KC.. Multiphase lattice Boltzmann simulations of buoyancy-induced flow of two immiscible fluids with different viscosities. European Journal of Mechanics B/Fluids 2012;34:105-114.

[6] Sahu KC, Vanka SP. A multiphase lattice Boltzmann study of buoyancy-induced mixing in a tilted channel. Computers & Fluids 2011;50:199-215.

[7] Hallez Y, Magnaudet J. Effects of channel geometry on buoyancy-driven mixing. Phys. Fluids 2008;20:053306.

[8] Séon T, Salin D, Hulin JP, Hinch EJ, Perrin B. Transient buoyancy-driven front dynamics in nearly horizontal tubes. Phys. Fluids 2007;19:123603.

[9] Séon T, Znaien J, Perrin B, Hinch EJ, Salin D, Hulin JP. Front dynamics and macroscopic diffusion in buoyant mixing in a tilted tube. Phys. Fluids 2007;19:125105.

[10] Baird MHI, Aravamudan K, Rao NVR, Chadam J, Pierce AP. Unsteady axial mixing by natural convection in a vertical column. AIChE J. 1992;38:1825-1834.

[11] Séon T, Hulin JP, Salin D, Perrin B, Hinch EJ . From turbulent mixing to gravity currents in tilted tubes. Phys. Fluids 2006;18:091103.

[12] Séon T, Hulin JP, Salin D, Perrin B, Hinch EJ . Laser-induced fluorescence measurements of buoyancy driven mixing in tilted tubes. Phys. Fluids 2006;18:041701.

[13] Séon T, Salin D, Hulin JP, Perrin B, Hinch EJ. Buoyant mixing of miscible fluids in tilted tubes. Phys. Fluids 2004;16(12);L103-L106.

[14] Séon T, Salin D, Hulin JP, Perrin B, Hinch EJ. Buoyancy driven miscible front dynamics in tilted tubes. Phys. Fluids 2005;17: 031702.

[15] Nasr-Azadani MM, Meiburg E. Turbidity currents interacting with three-dimensional seaoor topography. J. Fluid Mech 2014;745:409-443.

[16] Nasr-Azadani MM, Hall B, Meiburg E. Polydisperse turbidity currents propagating over complex topography: Comparison of experimental and depth-resolved simulation results. Comp. & Geosc. 2013;53:141-153.

[17] Hossain MA, Rees DaS. Natural convection flow of water near its density maximum in a rectangular enclosure having isothermal walls with heat generation. Heat and Mass Transfer 2005;41:367-374.

[18] Liu QS, Roux B, Velarde MG. Thermocapillary convection in two-layer systems. International Journal of Heat and Mass Transfer 1998;41:1499-1511.

[19] Prakash A, Koster JN. Steady natural convection in a two-layer system of immiscible liquids. International Journal of Heat and Mass Transfer. 1997;40:2799-2812.

[20] Villers D, Platten JK. Thermal convection in superposed immiscible liquid layers. Applied Scientific Research 1988;45:145-152.

[21] Watson A. The effect of the inversion temperature on the convection of water in an enclosed rectangular cavity. Journal of Mechanical and Applied Math. 1977:25:423-446

[22] Koster JN, Nguyen KY. Steady natural convection in a double layer of immiscible liquids with density inversion. International Journal of Heat and Mass Transfer 1996;39:467-478.

[23] Sahu KC, Ding H, Matar OK. Numerical simulation of non-isothermal pressure-driven miscible channel flow with viscous heating. Chemical Engineering Science 2010;65:3260-3267.

[24] Tripathi MK, Sahu KC, Govindarajan R. Why a falling drop does not in general behave like a rising bubble. Nature Scientific Reports 2014;4:4771.

[25] Redapangu PR, Sahu KC, Vanka SP. A study of pressure-driven displacement flow of two immiscible liquids using a multiphase lattice Boltzmann approach. Phys. Fluids 2012;24:102110.